https://doi.org/10.5194/egusphere-2025-6118
Preprint. Discussion started: 9 January 2026

Interpretable Machine Learning Quantifies Composition and Size Controls on Aerosol Spectral Absorption

Wenfang Wang[1], Pengfei Tian[1,2*], Shuhua Zeng[1], Yifei Zhang[1], Zeren Yu[1], Chen Cui[1], Yunfei Wu[3], Min Chen[1*], Lei Zhang[1,2]

[1] Key Laboratory for Semi-Arid Climate Change of the Ministry of Education, College of Atmospheric Sciences, Lanzhou University, Lanzhou 730000, China.

[2] Collaborative Innovation Center for Western Ecological Safety, Lanzhou University, Lanzhou 730000, China.

[3] State Key Laboratory of Atmospheric Environment and Extreme Meteorology, Institute of Atmospheric Physics, Chinese Academy of Sciences, Beijing 100029, China.

Corresponding author: P. Tian (tianpf@lzu.edu.cn) and M. Chen (chenmin@lzu.edu.cn)

https://doi.org/10.5194/egusphere-2025-6118
Preprint. Discussion started: 9 January 2026

Abstract

The spectral dependence of aerosol absorption, characterized by the absorption Ångström exponent (AAE), strongly influences radiative effects, yet the relative importance of controlling factors remains poorly quantified. We integrate multisource observations with an interpretable machine-learning framework (Shapley Additive Explanations, SHAP) to disentangle the roles of chemical composition and particle size in shaping AAE and to evaluate radiative impacts. Field observation in Beijing reveal that near-surface AAE is predominantly influenced by higher fine mineral dust and water-soluble inorganic ions fractions. Multi-year columnar data identify dust loading as the dominant factor, followed by carbonaceous aerosols. The fine-mode radius accounts for 29% of size parameters cumulative importance and ranks closely with black carbon. SHAP diagnostics highlight that columnar AAE contributes to radiative forcing at the top of the atmosphere (TOA) comparably to single scattering albedo (SSA), while its impact is clearly weaker at the bottom of the atmosphere and in the atmosphere. These findings help clarify AAE determinants and reduce uncertainties in aerosol radiative effect assessments.

https://doi.org/10.5194/egusphere-2025-6118
Preprint. Discussion started: 9 January 2026

1 Introduction

Light-absorbing aerosols (LAAs), primarily black carbon (BC), brown carbon (BrC), and mineral dust, significantly influence regional and global climate by absorbing solar radiation (Bahadur et al., 2012; Cappa et al., 2016; Kok et al., 2017; Nishant et al., 2019). For instance, BC contributed a net positive effective radiative forcing of 0.11 $W \cdot m^{-2}$ during 1750–2019, with a wide uncertainty range from –0.20 to +0.42 $W \cdot m^{-2}$ (Intergovernmental Panel On Climate Change (Ipcc), 2023), reflecting limited observational constraints on aerosol optical/microphysical properties and their inaccurate representation in models (Gliß et al., 2021; Lee et al., 2016). A practical diagnostic for the spectral shape of absorption is the Absorption Ångström Exponent (AAE) (Ångström, 1929; Lewis et al., 2008). For pure BC, AAE is theoretically close to 1.0, but observations show a range of 0.6–1.6 (Kirchstetter et al., 2004; Lack and Cappa, 2010; Gyawali et al., 2012; Chakrabarty et al., 2013; Wang et al., 2021). BrC and mineral dust exhibit relatively stronger absorption in the ultraviolet and visible spectral wavelengths, typically yielding AAE values greater than 2.0 (Russell et al., 2010; Park et al., 2018; Zhang et al., 2020; Cuesta-Mosquera et al., 2024). Because AAE encodes source and process information that governs aerosol absorption from ultraviolet to the near-infrared wavelength range, tighter constraints on AAE can help reduce uncertainties in aerosol radiative effects (Cazorla et al., 2013; Lack and Langridge, 2013; Sand et al., 2021).

https://doi.org/10.5194/egusphere-2025-6118
Preprint. Discussion started: 9 January 2026

AAE varies with particle size distribution, chemical composition, and mixing state (Scarnato et al., 2013; Li et al., 2016; Schuster et al., 2016a; Sotiropoulou et al., 2025). For instance, AAE may decrease as BC cores grow or as aggregates become more compact during aging processes (Liu et al., 2018). Recent numerical simulation further indicates that secondary organic coatings can increase AAE, with sensitivity to coating thickness (Zhang et al., 2025). In contrast, photochemical bleaching lowers BrC ultraviolet absorption and AAE (Wang et al., 2019; Li et al., 2025). Heterogeneous aging of long-range-transported dust may enhance absorption, also affecting AAE (Tian et al., 2018). The magnitudes and signs of these effects depend on location, season, and processing history, complicating both measurements and modeling and propagating to radiative forcing uncertainty (Sand et al., 2021; Li et al., 2022; Ponczek et al., 2022).

Studying the impact of individual factors on AAE is relatively straightforward. Previous studies have already examined the effects of particle size, chemical composition, and mixing state on AAE in isolation (Wu et al., 2015; Schuster et al., 2016b; Li et al., 2024). However, quantitatively attributing the relative contributions of particle size and chemical composition to AAE remains a challenging task due to nonlinearity and collinearity among predictors. For example, observations show that composition appears dominant when the shape of size distribution is quasi-stationary (Utry et al., 2014), whereas Mie-theory studies highlight the role of the imaginary refractive index of organics over size in explaining absorption changes (Yang et al., 2025). Although these studies effectively highlight the roles of particle size and

https://doi.org/10.5194/egusphere-2025-6118
Preprint. Discussion started: 9 January 2026

chemical composition, they lack quantitative assessments of their relative importance.

The Shapley Additive exPlanations (SHAP) method offers a principled framework for feature attribution in machine learning predictions and has been widely adopted in atmospheric sciences, such as boundary-layer height inversion, ozone formation and cloud-condensation-nuclei studies (Peng et al., 2023; Tao et al., 2024; Wang et al., 2025a). SHAP analysis has also been applied to aerosol absorption studies to precisely quantify the relative contribution of various chromophores to BrC absorption, providing a mechanistic understanding of its key drivers (Wang et al., 2024). Its potential to predict AAE and quantify the relative contributions of individual factors remains unexplored. Addressing this gap would offer an interpretable, data-driven perspective on aerosol spectral absorption.

This study aims to quantify the relative importance of chemical composition and particle size influencing AAE and to elucidate the critical role of AAE in radiative effects. We applied machine learning methods for columnar AAE (AAE_{col}), and assessed how AAE_{col} influences aerosol direct radiative forcing (ADRF) and aerosol radiative forcing efficiency (ARFE). During the modeling process, an ensemble of models was initially trained, after which the optimal model was selected to predict AAE_{col}, ADRF, and ARFE, with the SHAP algorithm used for interpretative analysis.

2 Methods

2.1 Field Campaign and Data Processing

https://doi.org/10.5194/egusphere-2025-6118
Preprint. Discussion started: 9 January 2026

An intensive observation campaign focusing on aerosol properties was conducted in urban Beijing, China, from 16 December 2023 to 15 January 2024. Online and offline instruments were deployed on the rooftop of the Institute of Atmospheric Physics, Chinese Academy of Sciences (Building #3; 39.98°N, 116.39°E), approximately 45 m above ground level. All online instruments were housed in a temperature-controlled room maintained at ~20 °C to ensure measurement stability, and sampling lines were equipped with Nafion dryers to minimize the influence of ambient humidity.

2.1.1 In Situ Online Aerosol Observations

Aerosol absorption coefficients ($b_{abs,\lambda}$) at 375, 532, and 870 nm were measured using photoacoustic extinctiometers (PAX, DMT Inc., USA). The PAX measures aerosol light absorption using the photoacoustic technique, in which absorbed laser energy is converted into periodic heating of the surrounding gas, generating an acoustic pressure wave in an acoustic resonator that is detected by a sensitive microphone (Truex and Anderson, 1979). The light absorption ($b_{abs,pax}$) can be calculated as:

$$b_{abs,pax} = \frac{P_{mic} \times A_{res} \times \pi^2 \times f_{res}}{P_L \times (\gamma - 1) \times Q} \quad (1)$$

where P_{mic} and P_L are the pressure of the microphone and the laser power, respectively; A_{res}, f_{res} and Q indicate the cross-sectional area, resonance frequency, and quality factor of the resonator; γ is the isobaric and isosteric specific heat ratio. Then the $b_{abs,\lambda}$ is obtained by subtracting the background absorption measured with particle-free air from $b_{abs,pax}$. In addition, the PAX measures aerosol scattering with an integrated wide-angle reciprocal nephelometer.

https://doi.org/10.5194/egusphere-2025-6118
Preprint. Discussion started: 9 January 2026

Prior to deployment, each PAX was calibrated following the procedure described in Wu et al., 2015: (i) the scattering channel was calibrated using high-concentration ammonium sulfate aerosol by regressing the extinction coefficient (b_{ext}) derived from laser power attenuation against the instrument-recorded scattering coefficient (b_{sca}). The scattering calibration factor was then adjusted by applying the regression slope as a multiplicative correction; (ii) the absorption channel was calibrated using high-concentration Aquadag aerosol by regressing (b_{ext} - b_{sca}) against the instrument-recorded photoacoustic absorption. The absorption calibration factor was then updated by dividing it by the regression slope.

The near-surface aerosol absorption Ångström exponent (AAE_{sfc}) was calculated as:

$$AAE_{sfc} = -\frac{\log(b_{abs,\lambda_1}) - \log(b_{abs,\lambda_2})}{\log(\lambda_1) - \log(\lambda_2)} \quad (2)$$

where λ_1 = 375 nm, λ_2 = 870 nm. Hourly $PM_{2.5}$ (particle matters with an aerodynamic diameter $\leqslant$ 2.5 μm) mass concentrations were obtained from the China National Environmental Monitoring Network for the Beijing urban site. These datasets were used to calculate mass absorption efficiency (MAE) of $PM_{2.5}$:

$$MAE_{\lambda} = \frac{b_{abs,\lambda}}{PM_{2.5}} \quad (3)$$

Size distributions were measured with a scanning mobility particle sizer (SMPS, Model 3082, TSI Inc., 8.8–310.6 nm, Stokes diameter) and an aerodynamic particle sizer (APS, Model 3321, TSI Inc., 0.54–19.8 μm, aerodynamic diameter), with SMPS data converted to aerodynamic diameter (Text S1) (Shang et al., 2018). To ensure

https://doi.org/10.5194/egusphere-2025-6118
Preprint. Discussion started: 9 January 2026

measurement accuracy, the flow systems of the SMPS and APS were periodically checked and calibrated by the manufacturer (TSI Inc.) through regular return-service calibration. In addition, hourly meteorological parameters (wind speed and direction, temperature, and relative humidity) were obtained from the 47 m meteorological tower at the Institute of Atmospheric Physics.

2.1.2 Offline Aerosol Sampling

Offline $PM_{2.5}$ samples were collected on quartz-fiber filters (90 mm diameter; Whatman 1855-090). Prior to sampling, quartz-fiber filters were pre-cleaned to minimize filter background. Briefly, filter cassettes were rinsed with absolute ethanol and air-dried, and aluminum-foil liners cut to the filter size were pre-baked at 550 °C for 3 h to remove residual carbon. The quartz filters were sequentially soaked in ultrapure water (5 min × 3 cycles, followed by 2 h × 2 cycles), oven-dried at 150 °C for 1 h, and then prebaked at 550 °C for 5 h to reduce the influence of adsorbed organic and inorganic materials. After cooling, the filters were wrapped in prebaked aluminum foil and conditioned for 48 h in a constant temperature and humidity environment prior to gravimetric determination. Then the pre-sampling filter mass was measured using an electronic microbalance (BSA124S-CW, Sartorius; readability ±0.1 mg). Sampling was conducted using a medium-volume air sampler (Model 2030, Laoshan Electronic Instrument Co., Ltd.) operated at 100 $L \cdot min^{-1}$ and equipped with a $PM_{2.5}$ inlet. The inlet was installed at approximately 2 m above ground level. Daytime samples were collected from 09:00 to 20:30, and nighttime samples from 21:00 to 08:30 the following day.

https://doi.org/10.5194/egusphere-2025-6118
Preprint. Discussion started: 9 January 2026

After sampling, all filters were analyzed for major chemical compositions, including water-soluble inorganic ions (Na^+, K^+, NH_4^+, Ca^{2+}, Mg^{2+}, Cl^-, NO_3^-, and SO_4^{2-}) measured by ion chromatography (881 Compact IC Pro, Metrohm; and ICS-1500, Dionex Inc.), metallic elements (Al, Ca, Mg, Fe, and Ti) determined by inductively coupled plasma–atomic emission spectrometry (ICP-AES; iCAP 7400, Thermo), and organic carbon (OC), and elemental carbon (EC) quantified using the thermal/optical carbon analyzer (DRI Model 2015, USA) based on the thermal/optical reflectance (TOR) method (Chow et al., 2007). The chemical analysis process is described in detail in Supplementary Text S2.

$PM_{2.5}$ was reconstructed as the sum of organic matter (OM=1.6×OC) (Guinot et al., 2007), EC, non-dust water-soluble ions (nd-WSII, and fine mineral dust (FMD) derived from crustal elements (Malm et al., 1994; Tian et al., 2023), showing good agreement with measured $PM_{2.5}$ (r = 0.82). Here, nd-WSII was defined as the sum of K^+, NH_4^+, NO_3^-, and SO_4^2, while Na^+, Ca^{2+}, Mg^{2+}, and Cl^- were excluded. Ca^{2+} and Mg^{2+} were treated as dust-related species, Na^+ was excluded due to generally elevated blanks associated with quartz-fiber filters and glassware, and Cl^- was excluded given its strong association with Mg^{2+} (r = 0.77, Table S1). The FMD was defined as follows:

$$[FMD] = 2.20[Al] + 2.49[Si] + 1.63[Ca] + 2.42[Fe] + 1.94[Ti] \quad (4)$$

where [Si] = 1.5 [Al].

2.2 Multiple Linear Regression

The influence of particle size and chemical composition on AAE_{sfc} was assessed

https://doi.org/10.5194/egusphere-2025-6118
Preprint. Discussion started: 9 January 2026

using a standardized multiple linear regression:

$$\widehat{AAE_{sfc}} = a + \mathrm{b} \times \widehat{\mathrm{FMD}} + \mathrm{c} \times \mathrm{nd}\widehat{-\mathrm{WSII}} + \mathrm{d} \times \widehat{\mathrm{D}_{SMPS}} + \mathrm{e} \times \widehat{\mathrm{D}_{APS}} \quad (5)$$

where $\widehat{AAE_{sfc}}$ denotes the standardized AAE_{sfc}; a represents the intercept term, encompassing EC, OM, and other potential influencing factors not explicitly accounted for; b, c, d, and e are regression coefficients; $\widehat{\mathrm{FMD}}$, $\mathrm{nd}\widehat{-\mathrm{WSII}}$, $\widehat{\mathrm{D}_{SMPS}}$, and $\widehat{\mathrm{D}_{APS}}$ are standardized variables of FMD fraction, nd-WSII fraction, and mean diameters from SMPS and APS, respectively. Offline chemical composition data were temporally matched to the corresponding online measurements based on sampling periods. Due to power outage on 27 December 2023 and 3 January 2024, daytime data for 27 December and both daytime and nighttime data for 3 January were unavailable.

2.3 AERONET Data

We used data from the Beijing Aerosol Robotic Network (AERONET) site (39.98° N, 116.38° E). Level 2.0 quality-assured Version 3 inversion products were selected. Key parameters include aerosol absorption optical depth (AAOD) at 440, 675, 870, and 1020 nm to calculate columnar AAE (AAE_{col}):

$$AAOD_{\lambda} = \mathrm{k} \times \lambda^{-AAE_{col}} \quad (6)$$

where k is a constant. In addition, aerosol size-related parameters were obtained, including volume size distributions for radii in the 0.05–15.00 μm range, mean radii of fine-mode and coarse-mode particles (R_{fine}, R_{coarse}), as well as volume concentrations of fine-mode (0.05–0.60 μm, vol_{fine}) (Sinyuk et al., 2020) and total particles (vol_{total}). The fine-mode fraction (FMF) was then calculated as:

https://doi.org/10.5194/egusphere-2025-6118
Preprint. Discussion started: 9 January 2026

$$FMF = \frac{vol_{fine}}{\mathrm{vol}_{total}} \quad (7)$$

To investigate the influence of chemical composition on AAE_{col}, we used the chemical composition dataset derived from AERONET inversions (Zhang et al., 2024), including black carbon (BC), brown carbon (BrC), coarse-mode absorbing soluble matter (CAI, representing coarse absorbing dust), coarse-mode non-absorbing soluble matter (CNAI, representing coarse non-absorbing dust and aged carbonaceous aerosols), and fine-mode non-absorbing soluble matter (FNAI, representing fine non-absorbing dust and organic carbon) (Zhang et al., 2024).

To further assess the radiative impacts of aerosols, we also employed AERONET shortwave instantaneous aerosol direct radiative forcing (ADRF) and aerosol radiative forcing efficiency (ARFE) data, where ARFE is defined as ADRF per unit aerosol optical depth (AOD) at 550 nm, reported at the top of the atmosphere (TOA), bottom of the atmosphere (BOA), and in the atmosphere (ATM) (Holben et al., 1998).

2.4 Shapley Additive Explanations (SHAP)

To quantify how particle size and chemical composition control the AAE_{col}, we trained and compared three ensemble tree–based regressors: Extreme Gradient Boosting (XGBoost), Random Forest (RF), and Categorical Boosting (CatBoost). Each model was trained using seven predictor variables, including five chemical compositions (BrC, BC, CAI, CNAI, and FNAI), and four size parameters (R_{fine}, R_{coarse}, vol_{fine}, and volume concentrations of coare-mode (vol_{coarse})). Model performance was evaluated using a consistent training–testing split and quantified by the coefficient of

https://doi.org/10.5194/egusphere-2025-6118
Preprint. Discussion started: 9 January 2026

determination (R^2), root mean square error (RMSE), and mean absolute error (MAE). The CatBoost model in our case was subsequently adopted for further interpretation (Fig. S7). SHapley Additive exPlanations (SHAP) analysis was applied to decompose the model output into additive feature contributions, enabling quantitative assessment of the relative contribution and sensitivity of individual aerosol composition and size parameters in determining. Predicted-versus-observed diagnostics are shown in Supplementary Fig. S7.

Similarly, to evaluate aerosol radiative impacts, XGBoost, RF, and CatBoost models also were trained using distinct predictor sets for different radiative metrics. For aerosol direct radiative forcing (ADRF), five optical properties (AOD, single scattering albedo (SSA), asymmetry parameter (g), surface albedo (SA), and AAE_{col}) were used as inputs. For radiative forcing efficiency (ARFE), the target definition (ARFE = ADRF/AOD) was kept unchanged; however, AOD was included during model fitting together with SSA, g, SA, and AAE_{col} so that the models could learn any residual nonlinearity and interactions involving AOD. Performance was again quantified by R^2, RMSE, and MAE on a consistent split. CatBoost in our case was retained as the best-performing model across TOA, BOA, and ATM. Predicted and observed comparisons are provided in Supplementary Fig. S8-S9.

To attribute ARFE variations while controlling for AOD, we employed SHAP with a scenario-based conditioning approach. Specifically, we recomputed SHAP values on the held-out test set after fixing AOD to four levels (25th, 50th, 75th percentiles, and

https://doi.org/10.5194/egusphere-2025-6118
Preprint. Discussion started: 9 January 2026

mean), computed from the training set to avoid information leakage, while leaving all other predictors unchanged. This yields SHAP attributions for SSA, g, SA, and AAE_{col} conditional on AOD at representative states. (The 50th percentile case is shown in the main text, others in Supplementary). For ADRF, SHAP was computed in the standard manner using all five predictors (AOD, SSA, g, SA, AAE） without conditioning.

3 Results and Discussion

3.1 Aerosol Characteristics During the Field Campaign

During the campaign, aerosol absorption decreased systematically with wavelength (375, 532, and 870 nm) (Fig. S2d), demonstrating typical wavelength-dependent characteristics. The corresponding mass absorption efficiencies were relatively low (0.49 ± 0.24, 0.21 ± 0.08, and 0.12 ± 0.04 $m^2 \cdot g^{-1}$), reflecting the dominance of nd-WSII, which accounted for 42.9% of $PM_{2.5}$ mass (Fig. 1a). Fig. 1a also showed that variations in near-surface AAE (AAE_{sfc}) were closely linked to changes in aerosol chemical composition mass fraction. Periods with elevated FMD fractions generally coincided with higher AAE_{sfc}, whereas intervals dominated by nd-WSII corresponded to lower values. The frequency distribution further indicates that AAE_{sfc} ranged from 0.90 to 3.0, and was most frequently 1.10–1.50 (mean 1.28 ± 0.39; Fig. 1b). Such elevated values likely resulted from winter heating emissions (Tian et al., 2019; Yan et al., 2017) and mineral dust contributions (Fig. 1a), both known to raise AAE (Liu et al., 2018).

https://doi.org/10.5194/egusphere-2025-6118
Preprint. Discussion started: 9 January 2026

Both absorption coefficients and AAE_{sfc} exhibited pronounced diurnal variability. Absorption coefficients were consistently higher absorption at night and a peak around 23:00 (Fig. S2), driven by reduced tropospheric boundary layer height, lower afternoon temperatures and wind speeds (Fig. S3), and enhanced emissions from nighttime traffic and heating(Guo et al., 2016; Zhao et al., 2019). AAE_{sfc} showed a clear night-high and day-low pattern, consistent with the evolution of particle size distributions. Fine-mode number concentrations derived from scanning mobility particle sizer (SMPS) increased during the morning rush hours and nighttime residential activity (Fig. 1c). By contrast, coarse-mode diameters from aerodynamic particle sizer spectrometer (APS) were larger in the early morning and decreased during the day (Fig. 1d). These results demonstrate that AAE_{sfc} was co-regulated by both composition and size, providing the observational evidence for the subsequent machine-learning analysis to quantify their relative contributions and radiative implications.

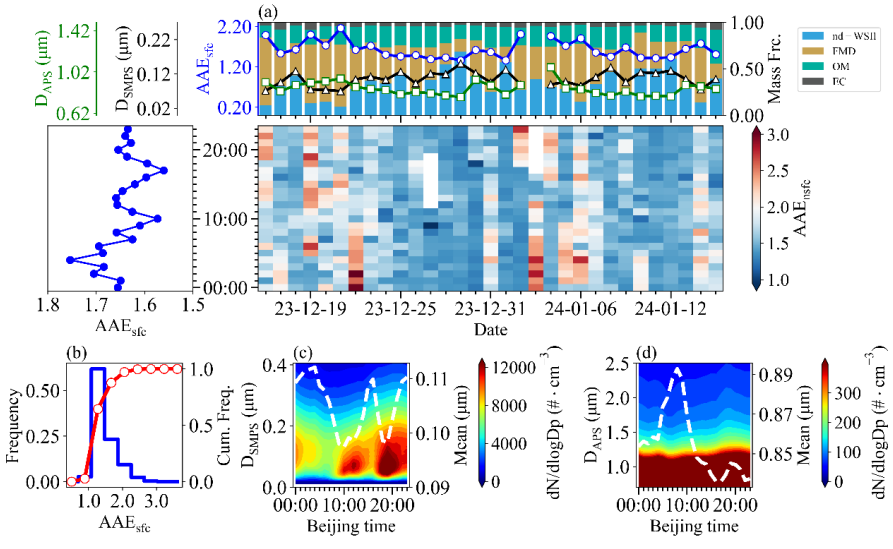

https://doi.org/10.5194/egusphere-2025-6118
Preprint. Discussion started: 9 January 2026

Figure 1. Aerosol absorption characteristics during the campaign. (a) Time series of mean particle diameters derived from SMPS and APS, mass fractions of organic matter (OM), elemental carbon (EC), non-dust water-soluble inorganic ions (nd-WSII), and fine mineral dust (FMD), together with daily averaged near-surface AAE (AAE_{sfc}). (b) Frequency distribution of AAE_{sfc}. (c–d) Diurnal variations of aerosol particle number size distributions from SMPS (c) and APS (d).

3.2 Influence of Composition and Size on Near-surface AAE

The EC mass fraction showed no correlation with AAE_{sfc} ($r = 0.09$, $p = 0.49$; Fig. 2a), which can be attributed to the weak wavelength dependence of EC absorption (Samset et al., 2018) and its relatively small mass contribution (~4%) (Fig. 2a). Similarly, the OM mass fraction is not significantly correlated with AAE_{sfc} ($r = -0.11$, $p = 0.40$; Fig. 2a). In contrast to study dominated by biomass burning, where light-absorbing organic carbon can account for > 50% of the mass fraction and strongly enhance AAE (Wang et al., 2021). During the Beijing campaign, however, OM contributed only ~19% of total $PM_{2.5}$ mass and BrC fractions were relatively low. Although BrC exhibits intrinsically high AAE values (Laskin et al., 2015; Moosmüller et al., 2011), its impact was diminished in the mixed aerosol matrix due to the influence of other dominant compositions.

We observed a statistically significant negative correlation between AAE_{sfc} and carbonaceous aerosol AAE (AAE_{CA}) (Fig. 2b), indicating that the non-carbonaceous aerosol had a significantly stronger role in shaping the absorption spectral dependence

https://doi.org/10.5194/egusphere-2025-6118
Preprint. Discussion started: 9 January 2026

under complex pollution conditions. Due to nitrogen dioxide (NO_2) concentrations were elevated at night (Fig. S4), which can interfere with PAX instruments, particularly at shorter wavelengths (Arnott et al., 2000; Gyawali et al., 2012). Therefore, we restrict the analysis here to daytime data (Fig S5). This pattern therefore cannot be ascribed simply to inter-instrument discrepancies.

AAE_{sfc} exhibited a significant positive correlation with the mass fraction of FMD ($r = 0.79$, $p < 0.01$) and a negative correlation with nd-WSII ($r = –0.78$, $p < 0.01$) (Fig. 2a). The AAE_{sfc} enhancement associated with FMD can be attributed to metal oxides such as hematite and goethite, which strongly absorb in the UV wavelengths and steepen the spectral dependence (Bi et al., 2016). By contrast, nd-WSII acted as non-absorbing diluents, suppressing the overall wavelength dependence. Although the "lensing effect" of nd-WSII can enhance the AAE_{CA} (Cappa et al., 2012; Zhang et al., 2025), due to the very low contribution of carbonaceous components to total $PM_{2.5}$ mass, preventing any observable positive correlation between AAE_{sfc} and the nd-WSII mass fraction.

Particle size also played a critical role. AAE_{sfc} was negatively associated with the fine-mode mean diameter from SMPS (D_{SMPS}, $r = –0.58$; Fig. 2c) and positively associated with the coarse-mode mean diameter from APS (D_{APS}, $r = 0.58$; Fig. 2d). Standardized multiple regression corroborated these effects, yielding coefficients of –0.02 for smaller particles and 0.44 for larger particles. Regression coefficients for composition were likewise consistent with the bivariate analysis: FMD had a positive

https://doi.org/10.5194/egusphere-2025-6118
Preprint. Discussion started: 9 January 2026

316 effect on AAE_{sfc} (coefficient is 0.35), whereas nd-WSII had a negative effect
317 (coefficient is –0.17). Particle size covaried with composition: D_{APS} was positively
318 correlated with the FMD mass fraction (r = 0.64) and negatively with nd-WSII (r = –
319 0.64), while D_{SMPS} was strongly positively correlated with nd-WSII (r = 0.89) and
320 negatively with FMD (r = –0.87) (Fig. S6). Together, these relationships indicate that
321 larger particles coincide with higher FMD and lower nd-WSII, enhancing AAE_{sfc},
322 whereas smaller particles favor inorganic salts and reduced dust contributions, lowering
323 AAE_{sfc}. Overall, AAE_{sfc} was not governed by carbonaceous aerosols alone but rather
324 by the coupled influence of mineral dust, inorganic matter, and particle size
325 distributions.

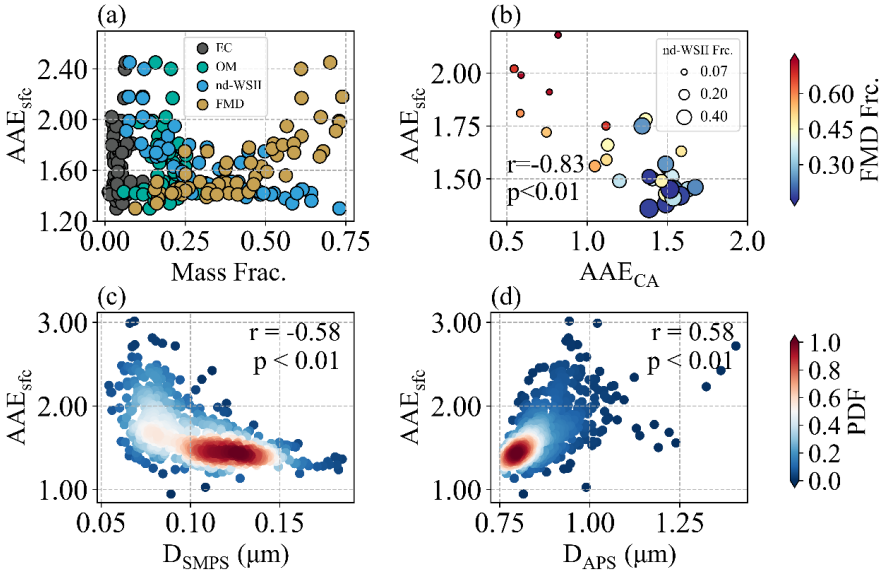

326

327 **Figure 2. Relationships of near-surface absorption Ångström exponent (AAE_{sfc})**
328 **with chemical composition and particle size.** (a) Scatter plots of chemical mass
329 concentration fraction and total aerosol AAE_{sfc}. (b) Relationship between AAE_{sfc} and

https://doi.org/10.5194/egusphere-2025-6118
Preprint. Discussion started: 9 January 2026

carbonaceous aerosol AAE (AAE_{CA}), with symbol size representing the non-dust water-soluble ions (nd-WSII) fraction and color denoting the fine mineral dust (FMD) fraction. (c–d) Correlations of AAE_{sfc} with mean particle diameters derived from SMPS (c) and APS (d), respectively. Shaded colors indicate probability density.

3.3 Quantitative Contributions of Composition and Size to Columnar AAE

The relationships between mass fractions of chemical composition and AAE_{col} were studied using AERONET data (Fig. 3). The AAE_{col} (1.47±0.56) was also suggested to be greater than that derived from the surface field campaign (Fig. 1), partially due to the vertical variation in aerosol absorption (Guan et al., 2024). The CNAI and FNAI mass fractions varied little and exhibited no significant correlations with AAE_{col} ($r = –0.03$ and 0.03, $p > 0.1$), indicating a negligible role in setting the absorption spectral dependence. In contrast, BC, BrC, and CAI displayed clear associations. Higher AAE_{col} (>1.5) were associated with marked increases in BrC and CAI, whereas lower AAE_{col} (<1.5) corresponded to relatively higher BC contributions. Correlation analysis is consistent with these patterns: AAE_{col} was negatively correlated with BC ($r = –0.19$, $p < 0.01$), in line with its weak wavelength dependence, but positively correlated with BrC ($r = 0.19$, $p < 0.01$) and CAI ($r = 0.31$, $p < 0.01$), underscoring the strong wavelength dependence of BrC and dust. These findings were similarly to our surface campaign, particularly regarding dust's amplifying effect on AAE_{col}.

https://doi.org/10.5194/egusphere-2025-6118
Preprint. Discussion started: 9 January 2026

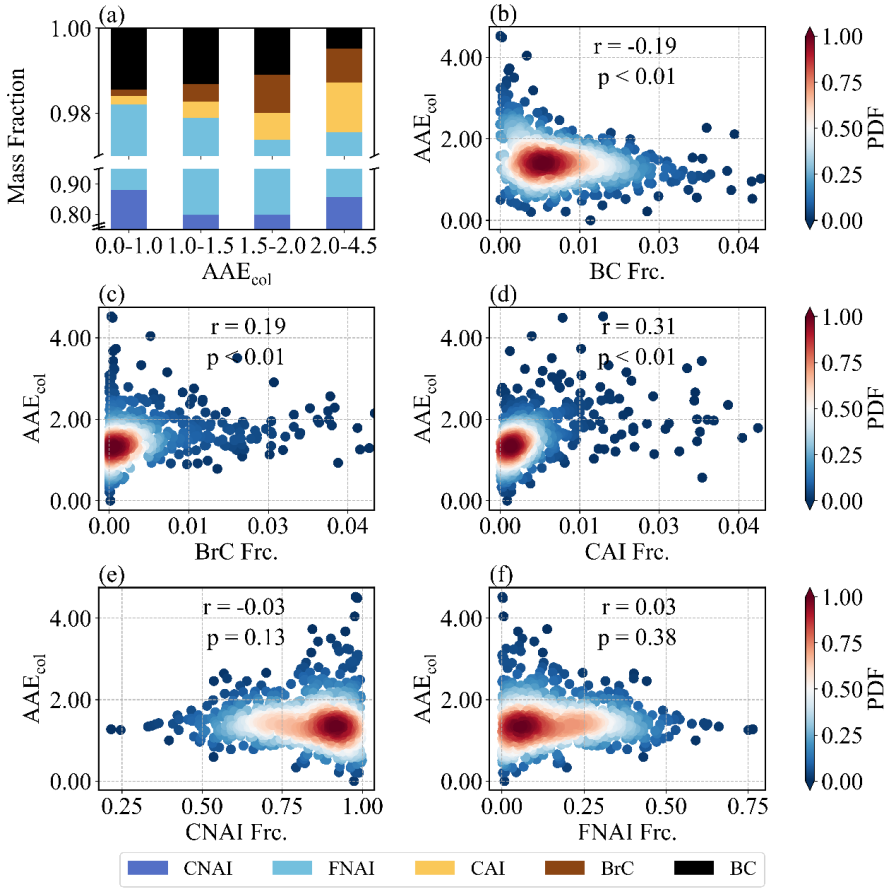

Figure 3. Relationships between columnar absorption Ångström exponent (AAE_{col}) and major aerosol chemical compositions. (a) Mass fractions of fine-mode non-absorbing soluble matter (FNAI), coarse-mode non-absorbing soluble matter (CNAI), coarse-mode absorbing soluble matter (CAI, representing dust), brown carbon (BrC), and black carbon (BC) across different AAE_{col} bins. (b-f) Correlations between AAE_{col} and the mass fractions of BC, BrC, CAI, CNAI, and FNAI, respectively; shaded colors denote probability density.

https://doi.org/10.5194/egusphere-2025-6118
Preprint. Discussion started: 9 January 2026

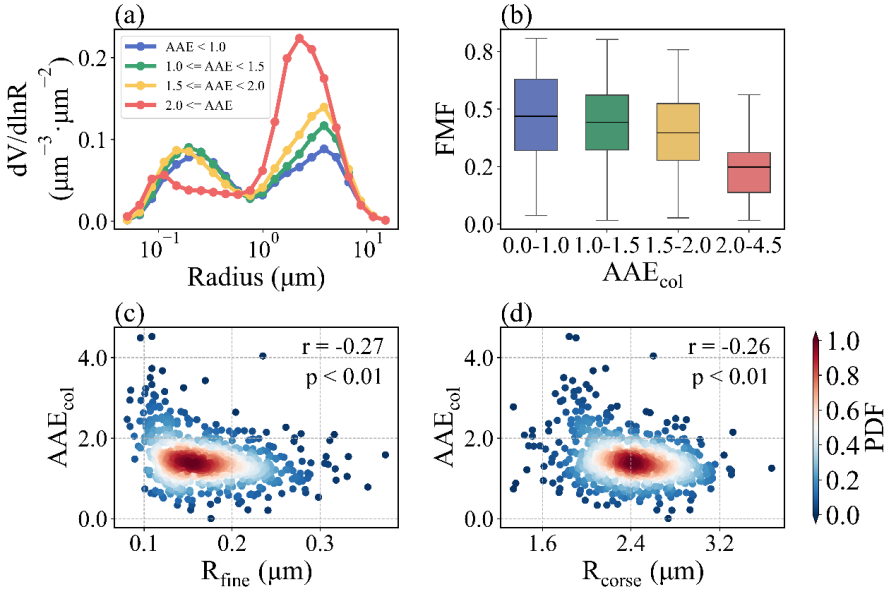

Figure 4. Relationships between columnar absorption Ångström exponent (AAE$_{col}$) and aerosol size distribution characteristics. (a) Volume size distributions grouped by AAE_{col} bins. (b) Fine-mode fraction (FMF) by AAE_{col} bins, with horizontal lines indicating means. (c–d) Correlations of AAE_{col} with effective radius of fine-mode (R_{fine}) and coarse-mode (R_{coarse}) particles, respectively.

The impacts of aerosol size distribution on AAE_{col} were clearly reflected (Fig. 4). With AAE_{col} increasing, the peaks of both fine and coarse modes shifted to smaller sizes, indicating an overall refinement of the size distribution. The R_{fine} and R_{coarse} were both negatively correlated with AAE_{col} ($r = –0.27$ and $–0.26$, $p < 0.01$), demonstrating that reductions in particle size in both modes enhanced the spectral dependence. Interestingly, FMF decreased with increasing AAE_{col}, suggesting that coarse-mode particles retained a substantial volumetric contribution even under high AAE_{col} conditions.

https://doi.org/10.5194/egusphere-2025-6118
Preprint. Discussion started: 9 January 2026

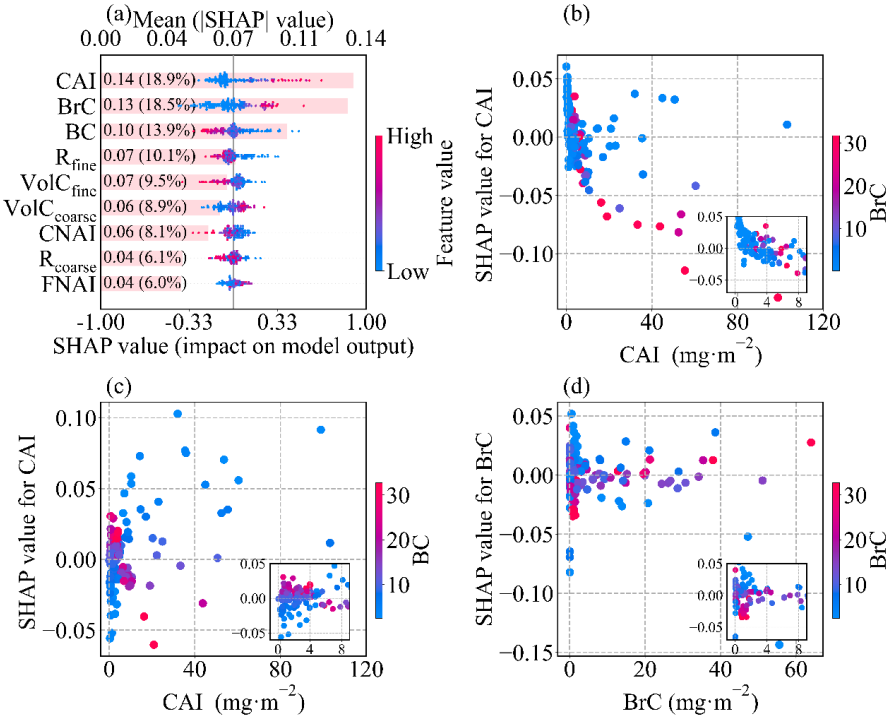

Figure 5. SHAP interpretation of the machine-learning model for columnar AAE. (a) Attribution of chemical compositions and particle size parameters to columnar AAE. Each horizontal bar represents the mean absolute SHAP value of a feature, indicating its overall impact on the model output; the color gradient shows the effect of feature values on columnar AAE, with red indicating a positive influence and blue indicating a negative influence. Features are ranked by importance. (b-c) SHAP dependence plots corresponding to CAI. (d) SHAP dependence plots corresponding to BrC.

Machine learning analysis further quantified relative contributions, as illustrated in Fig. 5a. It is found that showed that CAI had the strongest explanatory power, accounting for ~19% of the model performance, confirming the dominant role of dust in amplifying spectral absorption. BrC was second (18.5%) and BC was third (13.9%),

https://doi.org/10.5194/egusphere-2025-6118
Preprint. Discussion started: 9 January 2026

together with CAI explaining ~50% of model performance. Among the size-related predictors, R_{fine} alone accounted for about one quarter (~29%) of the cumulative importance of all size metrics, making it the most influential size parameter. Its importance was also clearly higher than CNAI and FNAI, indicating that the mean radius of fine-mode particles is the key size control on AAE_{col}. During the prediction process, it is observed that higher values of BrC, CAI, and volume concentrations of coare-mode (vol_{coarse}) corresponded to higher SHAP values and higher values of other predictors corresponded to smaller SHAP values. These responses are fully consistent with the correlations between AAE_{col} and these parameters (Fig. 3b–d; Fig. 4c-d). Collectively, these results demonstrated that AAE_{col} is not governed by BC or BrC alone; it is primarily modulated by dust and secondarily by particle-size structure (size metrics together ~35%), underscoring the need to account for both composition and size when evaluating spectral absorption.

To further investigate the interaction effects of major parameters on AAE_{col} prediction, we selected CAI, BrC, and BC, the three most influential predictors by SHAP, to analyze their interactions (Fig. 5b-5f). When CAI loading was below 10 $mg \cdot m^{-2}$, BrC suppressed the positive impact of CAI loading and progressively drove it toward a negative contribution. When CAI loading exceeded 10 $mg \cdot m^{-2}$, lower BrC is more likely than higher BrC to sustain or enhance the positive marginal effect of CAI, although the magnitude is weaker than in the CAI loading < 10 $mg \cdot m^{-2}$ regime. For CAI loading in the range 0–4, higher BC yielded a positive marginal effect of CAI on

https://doi.org/10.5194/egusphere-2025-6118
Preprint. Discussion started: 9 January 2026

AAE_{col}, whereas lowed BC yielded a negative one. Once CAI loading is greater than 4 $mg \cdot m^{-2}$, this relationship reverses, with higher BC more likely to make further increases in CAI contribute negatively to AAE_{col}. As BrC increases, BC progressively reduces the positive and negative contributions of BrC to AAE_{col}. These interactions indicate that models of aerosol spectral absorption should explicitly represent the mutual constraints among CAI, BrC, and BC to better identify and quantify AAE drivers.

3.4 Radiative Forcing and Efficiency Responses to Columnar AAE in Beijing

Joint analysis of the boxplots and SHAP diagnostics revealed a robust, layer-dependent coupling between the AAE_{col} and ADRF. As AAE_{col} increased from 0–1 to 2–4.5, cooling at the TOA intensifies, atmospheric heating weakened, and cooling at the BOA was alleviated (Fig. 6a-6c), reflecting a transition from BC-dominated, low-SSA conditions to high-SSA regimes influenced by BrC and mineral dust. SHAP method confirmed that AAE_{col} is the third strongest driver (~16%) after AOD (~56%), and comparably to SSA (~18%) at TOA and consistently shifts ADRF toward more negative values (Fig. 6d). At BOA, AAE_{col} contributes only ~4%. BOA cooling is primarily regulated by AOD (~65.0%) and SSA (~16 %) (Fig. 6e). In the ATM, AOD and SSA jointly dominated, but AAE_{col} still contributed comparably to surface albedo (SA) (both ~12%) (Fig. 6f), underscoring its role in vertically redistributing radiative energy. Mechanistically, higher AAE_{col} is associated with BrC and dust, which exhibit higher SSA but lower mass absorption efficiencies (MAE), thereby enhancing backscattering and solar escape (more negative TOA forcing), reducing absorption

https://doi.org/10.5194/egusphere-2025-6118
Preprint. Discussion started: 9 January 2026

(weaker atmospheric heating), and producing a net transmission effect that mitigates BOA cooling.

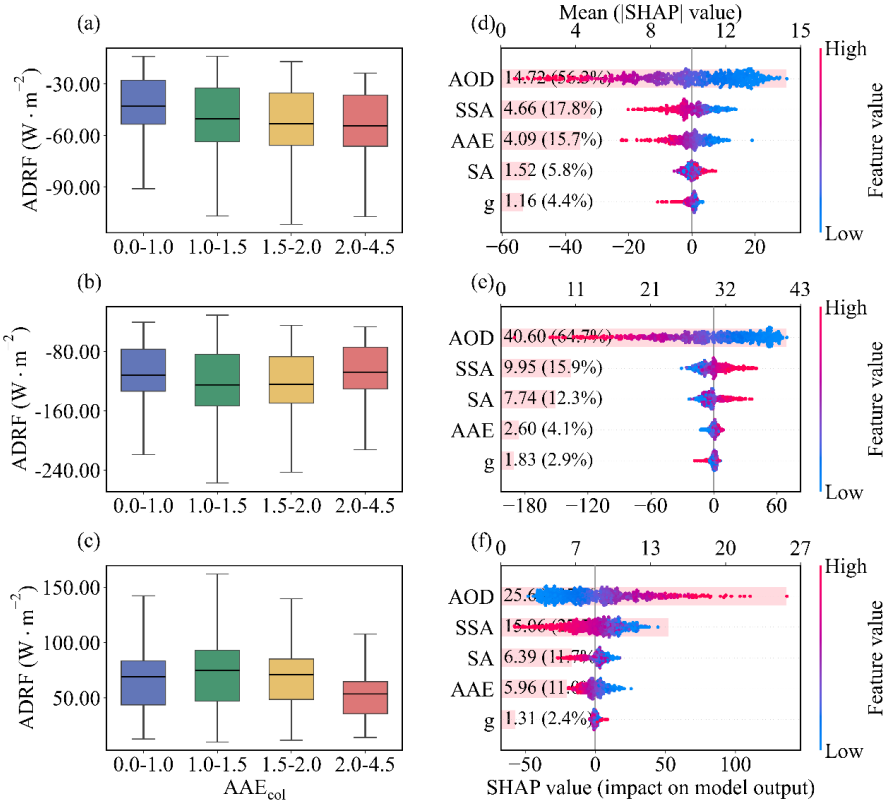

Figure 6. Role of columnar absorption Ångström exponent (AAE_{col}) in regulating aerosol direct radiative forcing (ADRF). (a–c) Box plots of ADRF at the top of the atmosphere (a), bottom (b), and in the atmosphere (c) as a function of AAE_{col}. (d–f) SHAP analysis quantifies the relative contributions of aerosol optical depth (AOD), single scattering albedo (SSA), asymmetry parameter (g), surface albedo (SA) and AAE_{col} in driving ADRF variations at the top of the atmosphere (d), at the bottom of the atmosphere (e), and in the atmosphere (f). The mean absolute SHAP values

https://doi.org/10.5194/egusphere-2025-6118
Preprint. Discussion started: 9 January 2026

436 (numbers in parentheses) indicate the relative contribution of each predictor to the
437 model output.

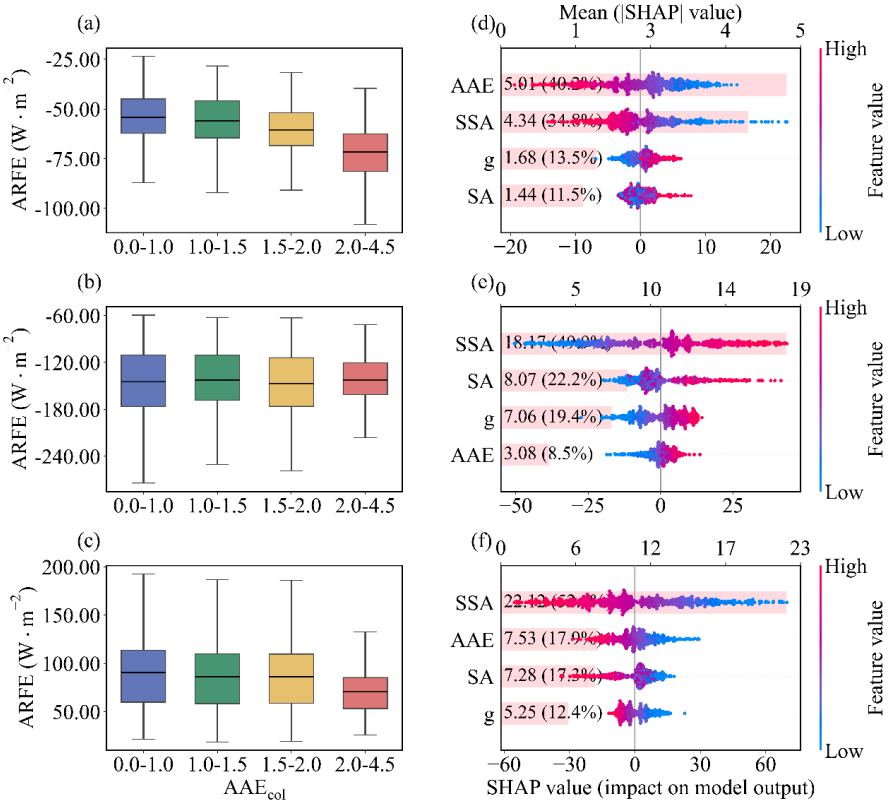

438

439 **Figure 7. Role of columnar absorption Ångström exponent (AAE_{col}) in regulating**
440 **aerosol radiative forcing efficiency (ARFE).** (a–c) Box plots of ARFE at the top of
441 the atmosphere (a), bottom (b), and in the atmosphere (c) as a function of AAE_{col}. (d–
442 f) SHAP analysis with AOD fixed at its median (50th percentile) quantifies the relative
443 contributions of single scattering albedo (SSA), asymmetry parameter (g), surface
444 albedo (SA) and AAE_{col} in driving ARFE variations at the top of the atmosphere (d),
445 bottom (e), and in the atmosphere (f). The mean absolute SHAP values (numbers in

https://doi.org/10.5194/egusphere-2025-6118
Preprint. Discussion started: 9 January 2026

parentheses) indicate the relative contribution of each predictor to the model output.

To better show columnar AAE's impact on ADRF, we introduced the ARFE, which removes the scaling by aerosol loading and highlights intrinsic optical controls. At TOA, AAE_{col} was the dominant driver of cooling efficiency based on mean |SHAP| (~40.0%), exceeding the asymmetry factor (g), SSA, and SA even when AOD was conditioned at 25th (Fig. S10), 50th (Fig. 7), 75th percentiles (Fig. S11), or mean (Fig. S12). Larger AAE_{col} was associated with more negative TOA ARFE, consistent with stronger shortwave backscattering by BrC and dust (Fig. 7d). At BOA, ARFE was governed primarily by SSA (~50%), followed by g and SA, with AAE_{col} contributing more modestly (~8%), increases in SSA and g tended to make ARFE less negative (Fig. 7e), indicative of enhanced forward scattering and greater transmittance for a fixed AOD. In the ATM, SSA dominated the heating-efficiency (>50%), with AAE_{col} and SSA providing secondary control (both ~17%), while g played a minor role (Fig. 7f). Higher AAE_{col} is linked to lower atmospheric heating efficiency, reflecting a shift toward aerosol types with weaker mass absorption than BC, and higher SSA further suppresses in-column absorption.

4 Conclusions

LAAs exert a strong influence on the Earth's radiation budget, yet the spectral dependence of their absorption, commonly summarized by the AAE, remains poorly constrained in urban regions. Here we combined in situ observation with long-term

https://doi.org/10.5194/egusphere-2025-6118
Preprint. Discussion started: 9 January 2026

AERONET column data and an interpretable machine-learning framework to disentangle the drivers of the AAE and to clarify its radiative implications.

Near the surface in wintertime Beijing, AAE variability co-varied primarily with enhanced fractions of fine mineral dust and water-soluble inorganic ions, underscoring that non-carbonaceous species can substantially modulate local absorption spectra in addition to BC and BrC. At the column level, SHAP diagnostics identified CAI as the leading driver of columnar AAE, followed by BrC and BC. Among particle size metrics, the fine-mode effective radius emerged as the most influential variable and accounted for about 29% of the cumulative importance of all size parameters, whereas non-absorbing composition (coarse and fine non-absorbing dust and non-absorbing carbonaceous aerosols) played only a minor role.

The radiative analysis shows that columnar AAE is a key regulator of ADRF at the TOA. Columnar AAE explained about 16% of the variance in TOA ADRF, comparable to the contribution from SSA, and became the leading predictor of TOA ARFE, accounting for roughly 40% of its variability and systematically enhancing TOA cooling efficiency. By contrast, the direct influence of AAE on ADRF and ARFE in the ATM and at the BOA was clearly weaker, where SSA and loading-related quantities remained dominant.

The findings of our study demonstrate the multifactorial control of AAE by composition and size and highlight its pivotal role in partitioning radiative forcing vertically among TOA, ATM, and BOA, especially at the TOA. Consequently,

https://doi.org/10.5194/egusphere-2025-6118
Preprint. Discussion started: 9 January 2026

accurately constraining AAE and its drivers is essential for a realistic representation of aerosol radiation interactions in regional and global models.

Data and code availability

The data that support the findings of this study are available in the Zenodo data repository (https://doi.org/10.5281/zenodo.17852818, Wang et al., 2025b). The AERONET data is freely available on the AERNOET website (https://aeronet.gsfc.nasa.gov/). The aerosol chemical composition derived from AERONET inversion data is available from https://doi.org/10.1175/BAMS-D-23-0260.1. The code scripts are also available in the Zenodo data repository (https://doi.org/10.5281/zenodo.17852818, Wang et al., 2025b).

Acknowledgments

We thank the AERONET PI at the Beijing site for their efforts in establishing and maintaining the site. We are also grateful to Prof. Yunfei Wu for providing access to the experimental facilities at the Institute of Atmospheric Physics, Chinese Academy of Sciences. We also thank the Lanzhou University Supercomputing Center for providing computational support.

Financial supports

This research was supported by the National Natural Science Foundation of China

https://doi.org/10.5194/egusphere-2025-6118
Preprint. Discussion started: 9 January 2026

505 (42475080), the Gansu Province Graduate Innovation Funding Project (2025CXZX-
506 177) and the Fundamental Research Funds for the Central Universities (lzujbky-2024-
507 ey04).

508 Author contribution

509 PT designed the study. PT and WW received the funding. WW, PT, SZ, ZY and
510 MC analyzed the data and led the writing. WW, YZ, YW and PT conducted the field
511 campaign. WW, PT, SZ, YZ, ZY, CC, YW, MC and LZ contributed to discussion, review,
512 and edit the manuscript.

513 Competing interests

514 The authors declare that they have no conflict of interest.

515 References

516 Ångström, A.: On the Atmospheric Transmission of Sun Radiation and on Dust in the
517 Air, Geografiska Annaler, 11, 156–166,
518 https://doi.org/10.1080/20014422.1929.11880498, 1929.
519 Arnott, W. P., Moosmüller, H., and Walker, J. W.: Nitrogen dioxide and kerosene-flame
520 soot calibration of photoacoustic instruments for measurement of light absorption
521 by aerosols, Review of Scientific Instruments, 71, 4545–4552,
522 https://doi.org/10.1063/1.1322585, 2000.

https://doi.org/10.5194/egusphere-2025-6118
Preprint. Discussion started: 9 January 2026

523 Bahadur, R., Praveen, P. S., Xu, Y., and Ramanathan, V.: Solar absorption by elemental
524 and brown carbon determined from spectral observations, Proc. Natl. Acad. Sci.
525 U.S.A., 109, 17366–17371, https://doi.org/10.1073/pnas.1205910109, 2012.
526 Bi, J., Huang, J., Holben, B., and Zhang, G.: Comparison of key absorption and optical
527 properties between pure and transported anthropogenic dust over East and Central
528 Asia, Atmos. Chem. Phys., 16, 15501–15516, https://doi.org/10.5194/acp-16-
529 15501-2016, 2016.
530 Cappa, C., Kotamarthi, R., Selacek, A., Flynn, C., Lewis, E., McComiskey, A., and
531 Riemer, N.: Absorbing Aerosols Workshop Report, January 20–21, 2016,
532 https://doi.org/10.2172/1471231, 2016.
533 Cappa, C. D., Onasch, T. B., Massoli, P., Worsnop, D. R., Bates, T. S., Cross, E. S.,
534 Davidovits, P., Hakala, J., Hayden, K. L., Jobson, B. T., Kolesar, K. R., Lack, D.
535 A., Lerner, B. M., Li, S.-M., Mellon, D., Nuaaman, I., Olfert, J. S., Petäjä, T.,
536 Quinn, P. K., Song, C., Subramanian, R., Williams, E. J., and Zaveri, R. A.:
537 Radiative Absorption Enhancements Due to the Mixing State of Atmospheric
538 Black Carbon, Science, 337, 1078–1081, https://doi.org/10.1126/science.1223447,
539 2012.
540 Cazorla, A., Bahadur, R., Suski, K. J., Cahill, J. F., Chand, D., Schmid, B., Ramanathan,
541 V., and Prather, K. A.: Relating aerosol absorption due to soot, organic carbon,
542 and dust to emission sources determined from in-situ chemical measurements,
543 Atmos. Chem. Phys., 13, 9337–9350, https://doi.org/10.5194/acp-13-9337-2013,

https://doi.org/10.5194/egusphere-2025-6118
Preprint. Discussion started: 9 January 2026

2013.

Chakrabarty, R. K., Arnold, I. J., Francisco, D. M., Hatchett, B., Hosseinpour, F., Loria, M., Pokharel, A., and Woody, B. M.: Black and brown carbon fractal aggregates from combustion of two fuels widely used in Asian rituals, Journal of Quantitative Spectroscopy and Radiative Transfer, 122, 25–30, https://doi.org/10.1016/j.jqsrt.2012.12.011, 2013.

Chow, J. C., Watson, J. G., Chen, L.-W. A., Chang, M. C. O., Robinson, N. F., Trimble, D., and Kohl, S.: The IMPROVE_A Temperature Protocol for Thermal/Optical Carbon Analysis: Maintaining Consistency with a Long-Term Database, Journal of the Air & Waste Management Association, 57, 1014–1023, https://doi.org/10.3155/1047-3289.57.9.1014, 2007.

Cuesta-Mosquera, A., Glojek, K., Močnik, G., Drinovec, L., Gregorič, A., Rigler, M., Ogrin, M., Romshoo, B., Weinhold, K., Merkel, M., Van Pinxteren, D., Herrmann, H., Wiedensohler, A., Pöhlker, M., and Müller, T.: Optical properties and simple forcing efficiency of the organic aerosols and black carbon emitted by residential wood burning in rural central Europe, Atmos. Chem. Phys., 24, 2583–2605, https://doi.org/10.5194/acp-24-2583-2024, 2024.

Gliß, J., Mortier, A., Schulz, M., Andrews, E., Balkanski, Y., Bauer, S. E., Benedictow, A. M. K., Bian, H., Checa-Garcia, R., Chin, M., Ginoux, P., Griesfeller, J. J., Heckel, A., Kipling, Z., Kirkevåg, A., Kokkola, H., Laj, P., Le Sager, P., Lund, M. T., Lund Myhre, C., Matsui, H., Myhre, G., Neubauer, D., Van Noije, T., North, P.,

https://doi.org/10.5194/egusphere-2025-6118
Preprint. Discussion started: 9 January 2026

565 Olivié, D. J. L., Rémy, S., Sogacheva, L., Takemura, T., Tsigaridis, K., and Tsyro,
566 S. G.: AeroCom phase III multi-model evaluation of the aerosol life cycle and
567 optical properties using ground- and space-based remote sensing as well as surface
568 in situ observations, Atmos. Chem. Phys., 21, 87–128,
569 https://doi.org/10.5194/acp-21-87-2021, 2021.
570 Guan, X., Tian, P., Wang, W., Zhang, M., Song, X., Zhang, Z., and Zhang, L.: More
571 Accurate Quantification of Direct Aerosol Radiative Effects Using Vertical
572 Profiles of Single-Scattering Albedo Derived From Tethered Balloon Observations,
573 JGR Atmospheres, 129, e2023JD040605, https://doi.org/10.1029/2023JD040605,
574 2024.
575 Guinot, B., Cachier, H., and Oikonomou, K.: Geochemical perspectives from a new
576 aerosol chemical mass closure, Atmos. Chem. Phys., 7, 1657–1670,
577 https://doi.org/10.5194/acp-7-1657-2007, 2007.
578 Guo, J., Miao, Y., Zhang, Y., Liu, H., Li, Z., Zhang, W., He, J., Lou, M., Yan, Y., Bian,
579 L., and Zhai, P.: The climatology of planetary boundary layer height in China
580 derived fromradiosonde and reanalysis data, Atmos. Chem. Phys., 16, 13309–
581 13319, https://doi.org/10.5194/acp-16-13309-2016, 2016.
582 Gyawali, M., Arnott, W. P., Zaveri, R. A., Song, C., Moosmüller, H., Liu, L.,
583 Mishchenko, M. I., Chen, L.-W. A., Green, M. C., Watson, J. G., and Chow, J. C.:
584 Photoacoustic optical properties at UV, VIS, and near IR wavelengths for
585 laboratory generated and winter time ambient urban aerosols, Atmos. Chem. Phys.,

https://doi.org/10.5194/egusphere-2025-6118
Preprint. Discussion started: 9 January 2026

12, 2587–2601, https://doi.org/10.5194/acp-12-2587-2012, 2012.

Holben, B. N., Eck, T. F., Slutsker, I., Tanré, D., Buis, J. P., Setzer, A., Vermote, E., Reagan, J. A., Kaufman, Y. J., Nakajima, T., Lavenu, F., Jankowiak, I., and Smirnov, A.: AERONET—A Federated Instrument Network and Data Archive for Aerosol Characterization, Remote Sensing of Environment, 66, 1–16, https://doi.org/10.1016/S0034-4257(98)00031-5, 1998.

Intergovernmental Panel On Climate Change (Ipcc): Climate Change 2021 – The Physical Science Basis: Working Group I Contribution to the Sixth Assessment Report of the Intergovernmental Panel on Climate Change, 1st ed., Cambridge University Press, https://doi.org/10.1017/9781009157896, 2023.

Kirchstetter, T. W., Novakov, T., and Hobbs, P. V.: Evidence that the spectral dependence of light absorption by aerosols is affected by organic carbon, J. Geophys. Res., 109, 2004JD004999, https://doi.org/10.1029/2004JD004999, 2004.

Kok, J. F., Ridley, D. A., Zhou, Q., Miller, R. L., Zhao, C., Heald, C. L., Ward, D. S., Albani, S., and Haustein, K.: Smaller desert dust cooling effect estimated from analysis of dust size and abundance, Nature Geosci, 10, 274–278, https://doi.org/10.1038/ngeo2912, 2017.

Lack, D. A. and Cappa, C. D.: Impact of brown and clear carbon on light absorption enhancement, single scatter albedo and absorption wavelength dependence of black carbon, Atmos. Chem. Phys., 10, 4207–4220, https://doi.org/10.5194/acp-

https://doi.org/10.5194/egusphere-2025-6118
Preprint. Discussion started: 9 January 2026

10-4207-2010, 2010.

Lack, D. A. and Langridge, J. M.: On the attribution of black and brown carbon light absorption using the Ångström exponent, Atmos. Chem. Phys., 13, 10535–10543, https://doi.org/10.5194/acp-13-10535-2013, 2013.

Laskin, A., Laskin, J., and Nizkorodov, S. A.: Chemistry of Atmospheric Brown Carbon, Chem. Rev., 115, 4335–4382, https://doi.org/10.1021/cr5006167, 2015.

Lee, L. A., Reddington, C. L., and Carslaw, K. S.: On the relationship between aerosol model uncertainty and radiative forcing uncertainty, Proc. Natl. Acad. Sci. U.S.A., 113, 5820–5827, https://doi.org/10.1073/pnas.1507050113, 2016.

Lewis, K., Arnott, W. P., Moosmüller, H., and Wold, C. E.: Strong spectral variation of biomass smoke light absorption and single scattering albedo observed with a novel dual-wavelength photoacoustic instrument, J. Geophys. Res., 113, 2007JD009699, https://doi.org/10.1029/2007JD009699, 2008.

Li, J., Liu, C., Yin, Y., and Kumar, K. R.: Numerical investigation on the Ångström exponent of black carbon aerosol, JGR Atmospheres, 121, 3506–3518, https://doi.org/10.1002/2015JD024718, 2016.

Li, J., Carlson, B. E., Yung, Y. L., Lv, D., Hansen, J., Penner, J. E., Liao, H., Ramaswamy, V., Kahn, R. A., Zhang, P., Dubovik, O., Ding, A., Lacis, A. A., Zhang, L., and Dong, Y.: Scattering and absorbing aerosols in the climate system, Nat Rev Earth Environ, 3, 363–379, https://doi.org/10.1038/s43017-022-00296-7, 2022.

https://doi.org/10.5194/egusphere-2025-6118
Preprint. Discussion started: 9 January 2026

628 Li, W., Riemer, N., Xu, L., Wang, Y., Adachi, K., Shi, Z., Zhang, D., Zheng, Z., and
629 Laskin, A.: Microphysical properties of atmospheric soot and organic particles:
630 measurements, modeling, and impacts, npj Clim Atmos Sci, 7, 65,
631 https://doi.org/10.1038/s41612-024-00610-8, 2024.
632 Li, Y., Fu, T.-M., Yu, J. Z., Zhang, A., Yu, X., Ye, J., Zhu, L., Shen, H., Wang, C., Yang,
633 X., Tao, S., Chen, Q., Li, Y., Li, L., Che, H., and Heald, C. L.: Nitrogen dominates
634 global atmospheric organic aerosol absorption, Science, 387, 989–995,
635 https://doi.org/10.1126/science.adr4473, 2025.
636 Liu, C., Chung, C. E., Yin, Y., and Schnaiter, M.: The absorption Ångström exponent
637 of black carbon: from numerical aspects, Atmos. Chem. Phys., 18, 6259–6273,
638 https://doi.org/10.5194/acp-18-6259-2018, 2018.
639 Malm, W. C., Sisler, J. F., Huffman, D., Eldred, R. A., and Cahill, T. A.: Spatial and
640 seasonal trends in particle concentration and optical extinction in the United States,
641 J. Geophys. Res., 99, 1347–1370, https://doi.org/10.1029/93JD02916, 1994.
642 Moosmüller, H., Chakrabarty, R. K., Ehlers, K. M., and Arnott, W. P.: Absorption
643 Ångström coefficient, brown carbon, and aerosols: basic concepts, bulk matter,
644 and spherical particles, Atmos. Chem. Phys., 11, 1217–1225,
645 https://doi.org/10.5194/acp-11-1217-2011, 2011.
646 Nishant, N., Sherwood, S. C., and Geoffroy, O.: Aerosol-induced modification of
647 organised convection and top-of-atmosphere radiation, npj Clim Atmos Sci, 2, 33,
648 https://doi.org/10.1038/s41612-019-0089-1, 2019.

https://doi.org/10.5194/egusphere-2025-6118
Preprint. Discussion started: 9 January 2026

649 Park, S., Son, S.-C., and Lee, S.: Characterization, sources, and light absorption of fine
650 organic aerosols during summer and winter at an urban site, Atmospheric Research,
651 213, 370–380, https://doi.org/10.1016/j.atmosres.2018.06.017, 2018.
652 Peng, K., Xin, J., Zhu, X., Wang, X., Cao, X., Ma, Y., Ren, X., Zhao, D., Cao, J., and
653 Wang, Z.: Machine learning model to accurately estimate the planetary boundary
654 layer height of Beijing urban area with ERA5 data, Atmospheric Research, 293,
655 106925, https://doi.org/10.1016/j.atmosres.2023.106925, 2023.
656 Ponczek, M., Franco, M. A., Carbone, S., Rizzo, L. V., Monteiro Dos Santos, D., Morais,
657 F. G., Duarte, A., Barbosa, H. M. J., and Artaxo, P.: Linking the chemical
658 composition and optical properties of biomass burning aerosols in Amazonia,
659 Environ. Sci.: Atmos., 2, 252–269, https://doi.org/10.1039/D1EA00055A, 2022.
660 Russell, P. B., Bergstrom, R. W., Shinozuka, Y., Clarke, A. D., DeCarlo, P. F., Jimenez,
661 J. L., Livingston, J. M., Redemann, J., Dubovik, O., and Strawa, A.: Absorption
662 Angstrom Exponent in AERONET and related data as an indicator of aerosol
663 composition, Atmos. Chem. Phys., 10, 1155–1169, https://doi.org/10.5194/acp-
664 10-1155-2010, 2010.
665 Samset, B. H., Stjern, C. W., Andrews, E., Kahn, R. A., Myhre, G., Schulz, M., and
666 Schuster, G. L.: Aerosol Absorption: Progress Towards Global and Regional
667 Constraints, Curr Clim Change Rep, 4, 65–83, https://doi.org/10.1007/s40641-
668 018-0091-4, 2018.
669 Sand, M., Samset, B. H., Myhre, G., Gliß, J., Bauer, S. E., Bian, H., Chin, M., Checa-

https://doi.org/10.5194/egusphere-2025-6118
Preprint. Discussion started: 9 January 2026

Garcia, R., Ginoux, P., Kipling, Z., Kirkevåg, A., Kokkola, H., Le Sager, P., Lund, M. T., Matsui, H., Van Noije, T., Olivié, D. J. L., Remy, S., Schulz, M., Stier, P., Stjern, C. W., Takemura, T., Tsigaridis, K., Tsyro, S. G., and Watson-Parris, D.: Aerosol absorption in global models from AeroCom phase III, Atmos. Chem. Phys., 21, 15929–15947, https://doi.org/10.5194/acp-21-15929-2021, 2021.

Scarnato, B. V., Vahidinia, S., Richard, D. T., and Kirchstetter, T. W.: Effects of internal mixing and aggregate morphology on optical properties of black carbon using a discrete dipole approximation model, Atmos. Chem. Phys., 13, 5089–5101, https://doi.org/10.5194/acp-13-5089-2013, 2013.

Schuster, G. L., Dubovik, O., and Arola, A.: Remote sensing of soot carbon – Part 1: Distinguishing different absorbing aerosol species, Atmos. Chem. Phys., 16, 1565–1585, https://doi.org/10.5194/acp-16-1565-2016, 2016a.

Schuster, G. L., Dubovik, O., Arola, A., Eck, T. F., and Holben, B. N.: Remote sensing of soot carbon – Part 2: Understanding the absorption Ångström exponent, Atmos. Chem. Phys., 16, 1587–1602, https://doi.org/10.5194/acp-16-1587-2016, 2016b.

Shang, D., Hu, M., Zheng, J., Qin, Y., Du, Z., Li, M., Fang, J., Peng, J., Wu, Y., Lu, S., and Guo, S.: Particle number size distribution and new particle formation under the influence of biomass burning at a high altitude background site at Mt. Yulong (3410 m), China, Atmos. Chem. Phys., 18, 15687–15703, https://doi.org/10.5194/acp-18-15687-2018, 2018.

Sinyuk, A., Holben, B. N., Eck, T. F., Giles, D. M., Slutsker, I., Korkin, S., Schafer, J.

https://doi.org/10.5194/egusphere-2025-6118
Preprint. Discussion started: 9 January 2026

691 S., Smirnov, A., Sorokin, M., and Lyapustin, A.: The AERONET Version 3 aerosol
692 retrieval algorithm, associated uncertainties and comparisons to Version 2, Atmos.
693 Meas. Tech., 13, 3375–3411, https://doi.org/10.5194/amt-13-3375-2020, 2020.
694 Sotiropoulou, R. E. P., Kaskaoutis, D. G., Kalkavouras, P., Grivas, G., Petrinoli, K.,
695 Garas, S. K., Liakakou, E., Tagaris, E., and Mihalopoulos, N.: Spatial variability
696 of carbonaceous aerosols and absorption characteristics between urban
697 background and residential sites during wintertime at a major Mediterranean city
698 (Athens; Greece), Atmospheric Research, 323, 108163,
699 https://doi.org/10.1016/j.atmosres.2025.108163, 2025.
700 Tao, C., Peng, Y., Zhang, Q., Zhang, Y., Gong, B., Wang, Q., and Wang, W.: Diagnosing
701 ozone–NO_x–VOC–aerosol sensitivity and uncovering causes of urban–
702 nonurban discrepancies in Shandong, China, using transformer-based estimations,
703 Atmos. Chem. Phys., 24, 4177–4192, https://doi.org/10.5194/acp-24-4177-2024,
704 2024.
705 Tian, J., Wang, Q., Ni, H., Wang, M., Zhou, Y., Han, Y., Shen, Z., Pongpiachan, S.,
706 Zhang, N., Zhao, Z., Zhang, Q., Zhang, Y., Long, X., and Cao, J.: Emission
707 Characteristics of Primary Brown Carbon Absorption From Biomass and Coal
708 Burning: Development of an Optical Emission Inventory for China, JGR
709 Atmospheres, 124, 1879–1893, https://doi.org/10.1029/2018JD029352, 2019.
710 Tian, P., Zhang, L., Ma, J., Tang, K., Xu, L., Wang, Y., Cao, X., Liang, J., Ji, Y., Jiang,
711 J. H., Yung, Y. L., and Zhang, R.: Radiative absorption enhancement of dust mixed

https://doi.org/10.5194/egusphere-2025-6118
Preprint. Discussion started: 9 January 2026

712 with anthropogenic pollution over East Asia, Atmos. Chem. Phys., 18, 7815–7825,
713 https://doi.org/10.5194/acp-18-7815-2018, 2018.
714 Tian, P., Zhang, N., Li, J., Fan, X., Guan, X., Lu, Y., Shi, J., Chang, Y., and Zhang, L.:
715 Potential influence of fine aerosol chemistry on the optical properties in a semi-
716 arid region, Environmental Research, 216, 114678,
717 https://doi.org/10.1016/j.envres.2022.114678, 2023.
718 Truex, T. J. and Anderson, J. E.: Mass monitoring of carbonaceous aerosols with a
719 spectrophone, Atmospheric Environment (1967), 13, 507–509,
720 https://doi.org/10.1016/0004-6981(79)90143-4, 1979.
721 Utry, N., Ajtai, T., Filep, Á., Pintér, M., Török, Zs., Bozóki, Z., and Szabó, G.:
722 Correlations between absorption Angström exponent (AAE) of wintertime
723 ambient urban aerosol and its physical and chemical properties, Atmospheric
724 Environment, 91, 52–59, https://doi.org/10.1016/j.atmosenv.2014.03.047, 2014.
725 Wang, N., Wang, Y., Lu, C., Zhu, B., Yan, X., Sun, Y., Xu, J., Zhang, J., and Shen, Z.:
726 Interpretable ensemble learning unveils main aerosol optical properties in
727 predicting cloud condensation nuclei number concentration, npj Clim Atmos Sci,
728 8, 302, https://doi.org/10.1038/s41612-025-01181-y, 2025a.
729 Wang, Q., Ye, J., Wang, Y., Zhang, T., Ran, W., Wu, Y., Tian, J., Li, L., Zhou, Y., Hang
730 Ho, S. S., Dang, B., Zhang, Q., Zhang, R., Chen, Y., Zhu, C., and Cao, J.:
731 Wintertime Optical Properties of Primary and Secondary Brown Carbon at a
732 Regional Site in the North China Plain, Environ. Sci. Technol., 53, 12389–12397,

https://doi.org/10.5194/egusphere-2025-6118
Preprint. Discussion started: 9 January 2026

https://doi.org/10.1021/acs.est.9b03406, 2019.

Wang, Q., Liu, H., Ye, J., Tian, J., Zhang, T., Zhang, Y., Liu, S., and Cao, J.: Estimating Absorption Ångström Exponent of Black Carbon Aerosol by Coupling Multiwavelength Absorption with Chemical Composition, Environ. Sci. Technol. Lett., 8, 121–127, https://doi.org/10.1021/acs.estlett.0c00829, 2021.

Wang, W., Tian, P., and Wu, Y.: Interpretable Machine Learning Quantifies Composition and Size Controls on Aerosol Spectral Absorption, https://doi.org/10.5281/ZENODO.17852818, 2025b.

Wang, Y., Huang, R.-J., Zhong, H., Wang, T., Yang, L., Yuan, W., Xu, W., and An, Z.: Predictions of the Optical Properties of Brown Carbon Aerosol by Machine Learning with Typical Chromophores, Environ. Sci. Technol., 58, 20588–20597, https://doi.org/10.1021/acs.est.4c09031, 2024.

Wu, Y., Yan, P., Tian, P., Tao, J., Li, L., Chen, J., Zhang, Y., Cao, N., Chen, C., and Zhang, R.: Spectral Light Absorption of Ambient Aerosols in Urban Beijing during Summer: An Intercomparison of Measurements from a Range of Instruments, Aerosol Air Qual. Res., 15, 1178–1187, https://doi.org/10.4209/aaqr.2014.09.0224, 2015.

Yan, C., Zheng, M., Bosch, C., Andersson, A., Desyaterik, Y., Sullivan, A. P., Collett, J. L., Zhao, B., Wang, S., He, K., and Gustafsson, Ö.: Important fossil source contribution to brown carbon in Beijing during winter, Sci Rep, 7, 43182, https://doi.org/10.1038/srep43182, 2017.

https://doi.org/10.5194/egusphere-2025-6118
Preprint. Discussion started: 9 January 2026

754 Yang, Z., Wang, Q., Wang, Q., Ma, N., Tian, J., Zhou, Y., Xu, G., Gao, M., Zhou, X.,
755 Zhang, Y., Ran, W., Yang, N., Tao, J., Hong, J., Wu, Y., Cao, J., Su, H., and Cheng,
756 Y.: Laboratory studies on the optical, physical, and chemical properties of fresh
757 and aged biomass burning aerosols, https://doi.org/10.5194/egusphere-2025-1020,
758 25 April 2025.
759 Zhang, X., Mao, M., Yin, Y., and Tang, S.: The absorption Ångstrom exponent of black
760 carbon with brown coatings: effects of aerosol microphysics and parameterization,
761 Atmos. Chem. Phys., 20, 9701–9711, https://doi.org/10.5194/acp-20-9701-2020,
762 2020.
763 Zhang, X., Li, L., Che, H., Dubovik, O., Derimian, Y., Holben, B., Gupta, P., Eck, T. F.,
764 Lind, E. S., Toledano, C., Xia, X., Zheng, Y., Gui, K., and Zhang, X.: Aerosol
765 Components Derived from Global AERONET Measurements by GRASP: A New
766 Value-Added Aerosol Component Global Dataset and Its Application, Bulletin of
767 the American Meteorological Society, 105, E1822–E1848,
768 https://doi.org/10.1175/BAMS-D-23-0260.1, 2024.
769 Zhang, Z., Wang, Y., Chen, X., Xu, L., Zheng, Z., Ching, J., Zhu, S., Liu, D., and Li,
770 W.: Absorption enhancement and shielding effect of brown organic coating on
771 black carbon aerosols, npj Clim Atmos Sci, 8, 102,
772 https://doi.org/10.1038/s41612-025-00989-y, 2025.
773 Zhao, S., Hu, B., Du, C., Tang, L., Ma, Y., Liu, H., Zou, J., Liu, Z., Wei, J., and Wang,
774 Y.: Aerosol optical characteristics and radiative forcing in urban Beijing,

https://doi.org/10.5194/egusphere-2025-6118
Preprint. Discussion started: 9 January 2026

775 Atmospheric Environment, 212, 41–53,

776 https://doi.org/10.1016/j.atmosenv.2019.05.034, 2019.

777